



## Intelligent hybrid system for dark spot detection using SAR data

Patrícia Genovez<sup>a,\*</sup>, Nelson Ebecken<sup>b</sup>, Corina Freitas<sup>a</sup>, Cristina Bentz<sup>c</sup>, Ramon Freitas<sup>d</sup>

<sup>a</sup> Brazilian Institute for Space Research, INPE – São José dos Campos, São Paulo, Brazil

<sup>b</sup> Federal University of Rio de Janeiro, COPPE/UFRJ, Rio de Janeiro - Brazil

<sup>c</sup> Research Center of Petrobras - CENPES , Rio de Janeiro - Brazil

<sup>d</sup> Camargo-Schubert Wind Engineering, Curitiba – Paraná - Brazil



### ARTICLE INFO

#### Article history:

Received 20 September 2016

Revised 16 March 2017

Accepted 17 March 2017

Available online 28 March 2017

#### Keywords:

Synthetic Aperture Radar

Digital Image Processing

Oil spills detection

Feature selection

Cluster analysis

Computational Intelligence

### ABSTRACT

Synthetic Aperture Radars (SAR) are the main instrument used to support oil detection systems. In the microwave spectrum, oil slicks are identified as dark spots, regions with low backscatter at sea surface. Automatic and semi-automatic systems were developed to minimize processing time, the occurrence of false alarms and the subjectivity of human interpretation. This study presents an intelligent hybrid system, which integrates automatic and semi-automatic procedures to detect dark spots, in six steps: (I) SAR pre-processing; (II) Image segmentation; (III) Feature extraction and selection; (IV) Automatic clustering analysis; (V) Decision rules and, if needed; (VI) Semi-automatic processing. The results proved that the feature selection is essential to improve the detection capability, keeping only five pattern features to automate the clustering procedure. The semi-automatic method gave back more accurate geometries. The automatic approach erred more including regions, increasing the dark spots area, while the semi-automatic method erred more excluding regions. For well-defined and contrasted dark spots, the performance of the automatic and the semi-automatic methods is equivalent. However, the fully automatic method did not provide acceptable geometries in all cases. For these cases, the intelligent hybrid system was validated, integrating the semi-automatic approach, using compact and simple decision rules to request human intervention when needed. This approach allows for the combining of benefits from each approach, ensuring the quality of the classification when fully automatic procedures are not satisfactory.

© 2017 Elsevier Ltd. All rights reserved.

## 1. Introduction

Remote sensing technologies have been widely accepted as effective providers of geospatial data to support oil and gas activities in offshore areas, from the exploration, until the production and transportation phases. During the last decades, the diversity of satellites operating in different spectral ranges, with multiple spatial resolutions and frequencies of acquisition were successfully applied to detect, map and monitor oil spills during routine or emergency situations (Brekke & Solberg, 2005; Engelhardt, 1999; Leifer et al., 2012; Topouzelis, 2008; API: American Petroleum Institute 2013; Fingas & Brown, 2014; IPIECA, 2014).

Particularly, Synthetic Aperture Radars (SAR) are consolidated as the main instrument to support the oil spill response (OSR), being delivered in near real time—sometimes—with a daily acquisition capability combining different microwave bands, resolutions, incidence angles and polarization modes. SAR provide cost effective

data, covering wide areas with synoptic surveys, during day and night, almost independent of weather conditions (Genovez, Freitas, Sant' Anna, Bentz, & Lorenzzetti, 2017; IPECA, 2014; Konik & Bradtke, 2016).

In the microwave spectrum, oil slicks are identified as dark spots, regions with low backscatter at sea surface. Despite SAR is being effectively used, oil spills detection still remains a challenge (Bentz, Politano, & Ebecken, 2012), due to the ambiguities caused by different biological, meteorological and oceanographic phenomena with backscatters similar to the oil, originating false alarms. Algae bloom, biological oils, low wind intensities, wind shadows, rain cells, upwelling, oceanic fronts, internal waves, suspended sediments as well as man-made occurrences as turbulent ship wakes, are examples of ambiguities frequently observed in SAR data.

Historically, trained interpreters are able to conduct the operational monitoring visually, distinguishing oil spills and look-alikes, as well as extracting the location and geometries of the slicks manually (Calabresi, Del Frate, Lichtenegger, Petrocchi, & Trivero, 1999; Fiscella, Giancaspro, Nirchio, Pavese, & Trivero, 2000; Mera, Bolon-Canedo, Cotos, & Alonso-Betanzos, 2017; Mera, Cotos, Varela-Pet, Rodríguez, & Caro, 2014; Solberg, Dokken, & Solberg,

\* Corresponding author.

E-mail addresses: [genovez.oilspill@gmail.com](mailto:genovez.oilspill@gmail.com) (P. Genovez), [nelson@ntt.ufrj.br](mailto:nelson@ntt.ufrj.br) (N. Ebecken), [corina@dpi.inpe.br](mailto:corina@dpi.inpe.br) (C. Freitas), [cris@petrobras.com.br](mailto:cris@petrobras.com.br) (C. Bentz), [aroramon@gmail.com](mailto:aroramon@gmail.com) (R. Freitas).

2003; Topouzelis, 2008). The multi-sensor approach together with contextual information regarding the platform position, pipelines, mono-buoys, ship routes and other potentially pollutant structures, are used as auxiliary information. This process is subjective, since it depends on the background and the experience of each interpreter. Additionally, when a large number of SAR scenes are available, the processing and human interpretation may be difficult and request a significant demand of time (Brekke & Solberg, 2005; Gade, Alpers, Hünerfuss, Wismann, & Lange, 1998; Indregard, Solberg, & Clayton, 2004; Keramitsoglou, Cartalis, & Kiranoudis, 2006; Solberg, Clayton & Indregard, 2005).

Automatic oil detection systems have been developed to optimize the processing time, to minimize the occurrence of false alarms and to reduce the subjectivity inherent to the human interpretation process, especially for large-scale monitoring efforts (Keramitsoglou, Cartalis, & Kiranoudis, 2006; Konik & Bradtke, 2016; Kubat, Holte, & Matwin, 1998; Espedal & Wahl, 1999; Mera et al., 2014; Solberg, 2005; Solberg et al., 2003; Topouzelis, 2008).

Four steps integrate the architectures planned for automatic oil detection systems: *i*) SAR pre-processing; *ii*) dark spot detection; *iii*) features extraction, and; *iv*) classification in oil or look-alikes (Angiuli, Frate, & Salvatori, 2006; Bjerde, Solberg, & Solberg, 1993; Brekke & Solberg, 2005; Chang, Cheng & Tang, 2005; Del Frate, Petrocchi, Lichtenegger, & Calabresi, 2000; Mera et al., 2014; Solberg et al., 2003; Topouzelis, 2008; Xu, Li, & Brenning, 2014; Zheng, Dong, Jiang, & Li, 2005). Particularly, the dark spot detection was investigated extensively due to of its importance inside the processing chain. The subsequent steps are thus influenced by the dark spots geometric accuracy, which determines the quality of the extracted features and, consequently, the performance of the classification in oil or look-alikes (Topouzelis, 2008; Topouzelis, Karathanassi, Pavlakis, & Rokos, 2007; Taravat & Oppelt, 2014).

In real conditions, SAR scenes provide simple scenarios with well-defined and easily detectable dark spots by automatic procedures, as well as complex scenarios with multiple dark spots occurring simultaneously in different scales, caused by oil spills together with look-alikes in different meteo-oceanographic conditions.

In all these situations, the contrast between the dark spots and the background determines the potential of the automatic systems to detect these events. This contrast is influenced by attributes related to the SAR systems, environmental conditions as well as characteristics of the spilled oils. Different bands, incidence angles, polarization, swath, speckle noise, low and high wind intensities, local sea state, type of oils slicks together with its drifting time and weathering stage (Brekke & Solberg, 2005; Gasull, Fabregas, Jimenez, Marques, Moreno, & Herrero, 2002; Holt, 2004; Montali, Giacinto, Migliaccio, & Gambardella, 2006; Solberg et al., 2005; Topouzelis, 2008; Zheng et al., 2005; Taravat & Oppelt, 2014; Konik & Bradtke, 2016; Marghany, 2014; Singha et al., 2014).

Part of the published research considers the methodologies developed as fully automatic but not operational, emphasizing the need of detailed tests, using a larger number of images, different types of dark spots including not well-defined slicks, influenced by different wind intensities and sea states (Brekke & Solberg, 2005; Karathanassi, Topouzelis, Pavlakis, & Rokos, 2006; Lopez, Moctezuma, & Parmiggiani, 2005; Mercier & Arduuin, 2005; Topouzelis, Stathakis, & Karathanassi, 2009).

Promising results obtained by dark spots with complex geometry and mixing oil spills with look-alikes are scarce, and the computational cost involved in these complex systems is mentioned as another factor that compromises its operational use (Gasull, Fabregas, Jimenez, Marques, Moreno, & Herrero, 2002; Karathanassi et al., 2006; Topouzelis et al., 2007).

Some approaches combined automatic and semi-automatic algorithms in different processing phases to improve the re-

sults (Calabresi et al., 1999; Fiscella et al., 2000; Angiuli et al., 2006; Chang et al., 2005; Frate et al., 2000; Lopez et al., 2005; Montali et al., 2006; Pelizzari & Dias, 2003; Singha, Velotto, & Lehner, 2014).

Summarizing, most methods declared as fully automatic achieve the greatest results when related to well-defined and well-contrasted dark spots over a homogeneous background (Taravat & Oppelt, 2014; Jing, He, FuKun, Jun Xia, & Hang, 2014), emphasizing the need to diversify and increase the number of tested samples to confer robustness to these methods.

There is an evident trade-off between automatic and semi-automatic methods. In one hand, the semi-automatic procedures have the potential of better results with higher confidence levels, but needing human intervention in different phases of the processing. On one hand, the fully automatic procedures are independent of the interpreter supervision and more adequate to treat a large dataset, but with a high computational cost. Additionally, when complex SAR scenes are acquired, the fully automatic systems may give back inaccurate geometries for the dark spots, compromising all subsequent processing steps.

Therefore, the operational use of fully automatic systems is not recommended to detect oil spills at sea surface. Human supervision is also required at the end of the process, as a way to provide quality control (Bentz et al., 2012; Konik & Bradtke, 2016; Singha et al., 2014; Solberg et al., 2005; Topouzelis, 2008; SeaSAR, 2010). This is more evident during emergencies where the data must be processed, interpreted and delivered promptly, with high confidence levels, avoiding contradictions to successfully support the decision makers planning the OSR and the strategies to protect vulnerable coastal areas (Garcia-Pineda et al., 2013).

In this context, this work presents an intelligent hybrid system, which is able to integrate automatic and semi-automatic procedures to detect dark spots at sea surface. Considering compact and simple decision rules, this system indicates the SAR scenes that could be automatically processed, returning acceptable geometric accuracy to be used as input for the classification in oil or look-alikes. At the end of the automatic processing, the semi-automatic procedure is integrated whether the decision rules consider that human intervention is needed to improve the dark spots geometry.

## 2. Intelligent hybrid system for dark spot detection

Six (6) steps compose the intelligent hybrid system proposed: (I) SAR pre-processing; (II) Image segmentation; (III) Feature extraction and selection; (IV) Automatic clustering analysis; (V) Decision rules and, if needed; (VI) Semi-automatic processing. This approach is illustrated in the flowchart (Fig. 1). An explanation about each step is available in the following items.

Considering the diversity of algorithms available to segment, select features and to cluster the data, there are many ways to construct an intelligent hybrid system as proposed here. This section presents a system construction and validation example for dark spots detection, integrating automatic and semi-automatic procedures by decision rules.

### 2.1. Dataset description and evaluation metrics

To construct a system example, a set of 12 SAR images acquired by RADARSAT-1 and RADARSAT-2 (C Band) in the ScanSAR Wide (SCW) and ScanSAR Narrow (SCN) beam modes was used, combining different spatial resolutions, swaths, incidence angles, polarizations and number of looks.

The scenes selection was done carefully in order to reflect, as consistently as possible, the real characteristics found in SAR data,

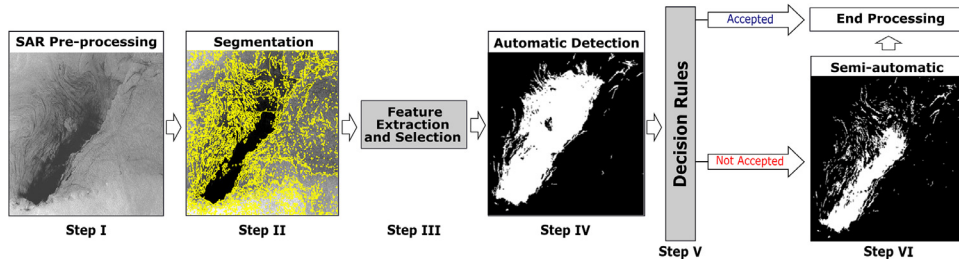


**Fig. 1.** Intelligent hybrid system integrating automatic and semi-automatic dark spot detection.

**Table 1**

SAR data description: characteristics of the selected subsets to develop the system.

SAR Subsets	Satellite	Date (DMY)	Beam Mode	Nº of Looks	Swath (km)	Pixel Spacing (m)	Polarization	Nº Dark Spots	Geometry	Scale	Contrast
1	RDS-1	06/07/2001	SCN	4	300	50	HH	1	Complex	Variable	Unstable
2	RDS-1	07/07/2001	SCN	4	300	50	HH	1	Simple	Invariable	Stable
3	RDS-1	06/03/2006	SCW	8	500	100	HH	1	Simple	Invariable	Unstable
4	RDS-1	09/09/2001	SCN	4	300	50	HH	Multiple	Simple	Variable	Unstable
5	RDS-2	13/06/2008	SCW	8	500	100	VV	Multiple	Both	Variable	Unstable
6	RDS-1	05/05/2002	SCN	4	300	50	HH	2	Simple	Invariable	Stable
7	RDS-1	19/12/2001	SCN	4	300	50	HH	1	Complex	Variable	Stable
8	RDS-1	03/04/2002	SCN	4	300	50	HH	Multiple	Complex	Variable	Stable
9	RDS-1	04/07/2001	SCN	4	300	50	HH	Multiple	Simple	Variable	Unstable
10	RDS-2	14/06/2008	SCN	4	300	50	VV	Multiple	Complex	Variable	Unstable
A	RDS-1	13/07/2007	SCW	8	500	100	HH	Multiple	Complex	Variable	Unstable
B	RDS-1	15/10/2001	SCN	4	300	50	HH	Multiple	Complex	Invariable	Stable

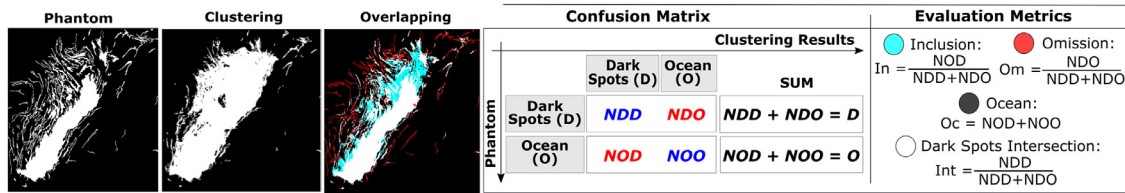


**Fig. 2.** Confusion matrix and metrics to evaluate the automatic and semi-automatic clustering results.

considering subsets with: *i*) Single dark spots, well-defined, well-contrasted and with simple geometry; *ii*) Multiple dark spots in different scales, with variable geometry; *iii*) Dark spots with low wind intensities in the background, and; *iv*) Gray level discontinuities eventually originated by processing failures in ScanSAR modes. Table 1 describes the characteristics of the selected dataset.

The evaluation procedure was completed overlapping the dark spots provided by the reference geometries, named Phantoms, with the clustering results (Fig. 2). The Phantoms are field-proven by Petrobras combining aircraft surveillance, visual observation, as well as satellite derived wind intensity and direction, chlorophyll concentration and sea surface temperature data. They were manually delineated by an experienced interpreter to produce a binary map, associating 0 to the ocean (background) and 1 to the dark spots. Thereby, the Phantoms may be considered as a field truth, indicating not only the nature of each dark spot, but providing the reference geometries.

As an overlapping result, a number of evaluation metrics are extracted from the confusion matrix (Fig. 2). The dark regions correctly clustered as dark regions are named NDD. The acronym NOO represents the ocean regions correctly merged as ocean. The dark regions erroneously clustered as ocean are indicated as NDO. Finally, the NOD refers to the ocean regions erroneously considered as dark regions.

The sum of NDD with NDO is equivalent to the dark spots, and the sum of NOO with NOD equals to the ocean, both of them de-

signed in the Phantoms. As shown in Fig. 2, the metrics of Intersection (In), Omission (Om) and Inclusion (In) are weighted by these dark spots reference, represented in its denominators by the sum of NDD with NDO.

The Omission (Om) is considered the most significant and critical metric to guide the oil spill response actions (OSR). When overlapped with the Phantoms reference, the Omission indicates how the classification failed to cluster dark regions as ocean, damaging the dark spots geometry. In its worst case, the Om may not detect an oil spill, which compromises and delays the planning and implementation of the OSR, increasing the environmental impacts.

In contrast, the Inclusion (In) metric may cause an overestimation of the occurrence. However, it is better to make a mistake by generating a false alarm than by excluding a real emergency.

The Fraction of Intersection (Int) between the Phantoms and the clustering results indicates the proportion of the dark regions correctly clustered as dark spots. This metric, previews the proportion of the dark spots mapped as indicated by the Phantoms, however it does not consider the inclusion errors.

In this way, the main evaluation metric proposed is named Dark Spot Accuracy (DSA), which aims to weigh the regions correctly classified by all types of errors (Genovez, 2010). The equation below represents the metric concept:

$$DSA = \frac{NDD}{NDD + NDO + NOD} \quad (1)$$

Values of DSA near 1 indicate that the clustered dark spots are more similar to those designed by the Phantom. The DSA indexes greater than or equal to 0.50 are considered satisfactory (S) and DSA lower than 0.50 are considered unsatisfactory (US). These criteria were defined considering the interpreters experience. The statistical significance of the results used the non-parametric Wilcoxon test, considering  $p$ -levels below 0.05 as significant.

It is important to highlight that the Phantoms were used only to construct and validate the intelligent hybrid system, allowing to evaluate the algorithms applied and the features selected. In this context, in a real operational system, the Phantoms construction is not necessary.

## 2.2. SAR pre-processing and segmentation

Considering the diversity of SAR sensors currently available, operating in different bands with different spatial resolutions, swaths, incidence angles and polarization modes, the pre-processing is an important step, especially to treat dataset in large-scale monitoring initiatives.

SAR scenes with different levels of complexity, should be pre-processed (Step I) in order to georeference the data and to remove the antenna pattern effect. Another important pre-processing step is the speckle noise minimization inherent to the SAR systems, using proper filters and adequate window size.

During the segmentation process (Step II), the images are partitioned into regions considering homogeneity and heterogeneity criteria. The algorithms can be organized into 3 categories: *i*) Region fitting; *ii*) Edge-based, and; *iii*) Region-growing (Navulur, 2007). The region-fitting and the edge-based algorithms return results to pixel level, while the region-growing algorithms merge the pixels into regions. Especially for the SAR data applications, the region growing is recommended (Silva, Câmara, Souza, Valeriano, & Escada, 2005) which is able to reduce the interference of the speckle noise in the dark spot detection results (Chang et al., 2005; Galland, Réfrégier, & Germain, 2004; Konik & Bradtk, 2016).

The images were pre-processed with 100 m pixel spacing (Hang & Dinh, 2009). Different authors also indicated this resolution as adequate, functioning as a primary filter and, smoothing the SAR inherent noise (Brekke & Solberg, 2005; Calabresi et al., 1999; Fiscella et al., 2000; Del Frate et al., 2000; Gasull, Fabregas, Jimenez, Marques, Moreno, & Herrero, 2002; Bentz, 2006; Genovez, 2010; Keramitsoglou, Cartalis, & Kiranoudis, 2006).

Genovez (2010) tested eight (8) SAR speckle filters considering window sizes  $3 \times 3$ ,  $5 \times 5$  and  $7 \times 7$ . The Lee  $3 \times 3$  provided better results and was used here to filter the SAR scenes. This filter was successfully applied in other studies to pre-process the SAR images to detect oil spills (Hang & Dinh, 2009; Karathanassi et al., 2006; Stathakis, Topouzelis, & Karathanassi, 2006; Topouzelis et al., 2007; Topouzelis et al., 2009).

The subsets were segmented using a region-growth algorithm developed at the Brazilian Institute for Space Research – INPE, named ISOSEG (Bins, Fonseca, & Erthal, 1996; Câmara et al., 1996). The ISOSEG was used to split the images into regions, considering as parameters the minimum area equivalent 25 pixels and the similarity threshold 4. The minimum area was defined considering Petrobras experience to detect oil spills at sea surface on board inspection flights visually. According to the technical reports over the last 6 years, the minimum area estimated and detected was about 0.25 km<sup>2</sup>. Considering 100 m of pixel spacing, 25 pixels would be enough to detect an equivalent area.

## 2.3. Feature extraction

In previous works of several authors, different numbers and types of features have been used to detect oil slicks at sea sur-

face. Solberg and Theophilopoulos (1997) extracted 15 features, Solberg et al. (1999) tested 11 features, Fiscella et al. (2000) and Keramitsoglou, Cartalis, & Kiranoudis, (2006) referred to 14 features, Karathanassi et al. (2006) used 13 features, Bentz, Ebecken, and Politano (2007) calculated 40 including contextual and meteorological attributes. Several studies (Topouzelis et al., 2009 & Bentz et al., 2012; Stathakis et al., 2006; Konik & Bradtk, 2016) synthesized the most commonly 25 features used in the published researches. Recently, Chehresa et al. (2016) used 74 features and Mera, Bolon-Canedo, Cotos, Alonso-Betanzos (2017) evaluated 52 features. Although the number of features may vary, the main attributes extracted are distributed in the following categories: *i*) Statistical: based on backscatter values; *ii*) Textural: calculated considering the gray level co-occurrence matrix (Haralick, Shanmugan, & Dinstein, 1973); *iii*) Geometrical: extracted from the geometry of polygons (Definiens Professional 5 2006), and; *iv*) Polarimetric: calculated according to the available polarization mode (Skrunes, Brekke, Eltoft, Kudryavtsev, 2015; Migliaccio, Nunziata, & Buono, 2015).

To develop the proposed system, 36 thirty six (36) predictor features (PF) were extracted from 10 SAR subsets (Table 2), being: *(i)* eight (8) statistical; *(ii)* eight (8) textural, extracted from the Grey Level Co-occurrence Matrix (GLCM), and; *(iii)* twenty (20) geometrical features. Considering that the PF have different value ranges, a linear normalization was applied. As the dark spots geometry is quite variable depending of their nature, a greater number of geometrical attributes was tested, increasing the number of features.

To select the most promising set of features, the 36 predictor features were analyzed in a controlled way, using as reference a dependent variable named Phantom Class (PC). The PC assigns one category to each segmented region, considering as field truth the classes pre-defined in the Phantoms. However, since an over-segmentation is frequent, the Phantom borders do not coincide with the segmented borders. Generally, more than one segment is generated per dark spot.

The solution was to use one continuous range from 0 to 1, indicating the percentage that each segmented region intersects the dark spots geometry in the Phantom, considering 4 classes: *i*) Ocean Region: lower than 25%; *ii*) Transition between Ocean and Dark Region: between 25% and 50%; *iii*) Transition between Dark and Ocean Region: between 50% and 75%, and; *iv*) Dark Region: more than 75% intersection. Fig. 3 illustrates the method applied to assign the classes into the segmented regions.

It is interesting to mention that, in previous research, the feature extraction and its selection were commonly used to improve the classification results in oil or look-alikes (Aggarwal, 2015; Bentz et al., 2007; Karathanassi et al., 2006; Kubat, Holte, & Matwin, 1998; Stathakis et al., 2006; Topouzelis et al., 2009; Topouzelis et al., 2012; Xu et al., 2014). However, the approach proposed here aims to evaluate the contribution of different features to improve the dark spot detection.

## 2.4. Feature selection

Feature selection is recommended to find the best set of features, which characterizes the original dataset, removing unnecessary, irrelevant, redundant or noisy variables (Lehmann & Joseph, 2005; Liu & Setiono, 1995; Stathakis et al., 2006). Fewer features may reduce the complexity of the models, could improve the quality of the dataset and, consequently, increase the accuracy of the dark spots detection (Aggarwal, 2015; Bentz et al., 2007; Duda, Hard, & Stork, 2000; Mera et al., 2017).

There are three possibilities to integrate the feature selection step in one automatic system: *i*) pre-defining the system input features; *ii*) selecting the best set of features for each new image, and;

**Table 2**  
Predictor features extracted from the segmented regions.

Statistical	
1 Mean: Me	5 Minimum: Min
2 Standard Deviation: Sd	6 Asymmetry: As
3 Median: Md	7 Kurtosis: Kt
4 Maximum: Max	8 Mode: Mo
Textural	
9 GLCM: Angular Second Moment	13 GLCM: Entropy
10 GLCM: Contrast	14 GLCM: Homogeneity
11 GLCM: Correlation	15 GLCM: Mean
12 GLCM: Dissimilarity	16 GLCM: Standard Deviation
Geometrical	
17 Area	27 Average Length of Edges (Polygon)
18 Length	28 Length of Longest Edge (Polygon)
19 Width	29 Compactness (Polygon)
20 Border Length	30 Degree of Skeleton Branching
21 Asymmetry	31 Length of Main Line
22 Density	32 Length of Main Line (Regarding Cycles)
23 Shape Index	33 Length/Width (Only Main Line)
24 Elliptic Fit	34 Maximum Branch Length
25 Rectangular Fit	35 Stddev of Length of Edges (Polygon)
26 Compactness	36 Width (Only Main Line)

\*GLCM: Gray Level Co-occurrence Matrix.

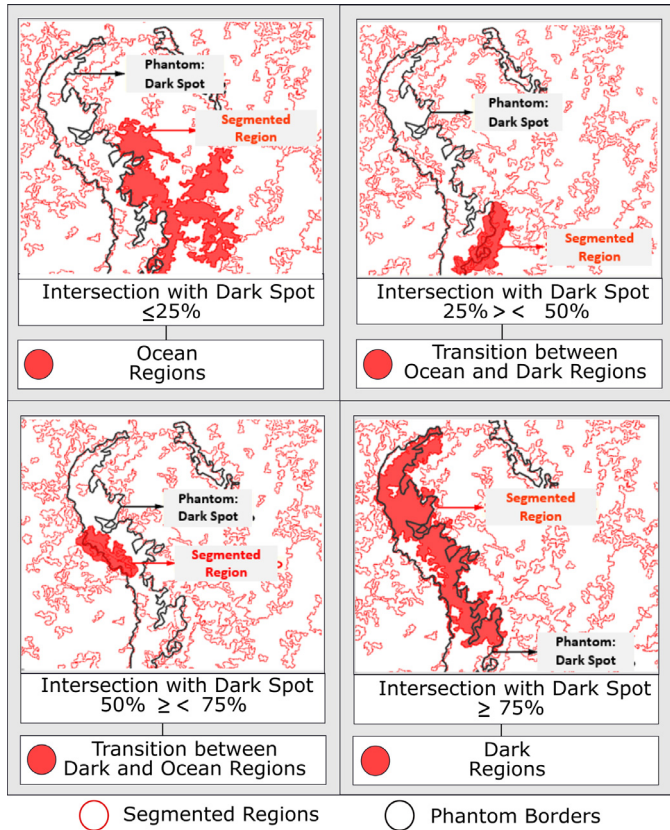


**Fig. 3.** Criteria used to assign the classes, Dark spot and ocean, into the segmented regions creating the Phantom Class feature.

put features. This process was done analyzing the 36 predictor features regarding the dependent variable Phantom Class (PC).

The feature selection methods can be divided in three categories (Aggarwal, 2015; Lehmann & Joseph, 2005; Qian, Shu, & Zhang, 2016; Vanaja & Kumar, 2014): Filter, Wrapper and Hybrid methods. Filter methods use a similarity-based criterion to provide one ranking of features according to its importance. These methods consider the features independently or regarding the dependent feature. The Information Gain, Gini Index, Measures of Discrepancy and Chi-square test are examples of Filter Methods. Wrapper methods use an internal validity criterion integrated with a clustering algorithm to evaluate an appropriate subset of features. At this approach, different subsets of features must to be explored to determine the optimum combination of features, being sensitive to the validity criterion and the clustering algorithm chosen. The recursive feature elimination algorithm is a wrapper method example. Hybrid methods combine the advantages of both mentioned methods to improve the feature selection accuracy. The wrapper methods are dependent on the chosen clustering method, returning a different set of features for different cluster algorithms, while the filter methods can be performed independently as a pre-processing phase, requiring less processing time (Liu & Setiono, 1995; Qian et al., 2016; Vanaja & Kumar, 2014).

The filter method named Variable Screening (VS), based on Chi-square test, was chosen to find the best set of predictor features better related with the dependent feature Phantom Class (PC). Filter methods like the VS are recognized as effective and reliable to select features in large datasets, processing numerical and categorical features simultaneously, without assuming a linear or a monovariate relationship between the predictors and the dependent variable (Liu & Setiono, 1995; Qian et al., 2016; Vanaja & Kumar, 2014). Therefore, the Variable Screening method was used to perform the feature selection. As a result, the algorithm provides a ranking of predictor features in decreasing order, considering the statistical significance (*p*-value) calculated for each chi-square value.

To strengthen the chosen method, some experimental results obtained by the adopted Variable Screening were compared with other methods like Genetic Algorithm (GA) and Greedy Stepwise (GS), as indicated in Fig. 4. This comparison was completed using

iii) choosing the best set of features for each new image interactively, by pattern recognition techniques and using a knowledge database with constant feedback of new examples. In this system construction example, the feature selection was used to identify the most promising attributes, aiming to pre-define the set of in-

**Table 3**  
Ranking of 10 first features selected by the variable screening per subset.

	Subset 1	Subset 2	Subset 3	Subset 4	Subset 5
1°	Mean	Density	Median	Mode	Median
2°	Median	Maximum	Mean	Median	Mode
3°	Mode	Minimum	Minimum	Mean	Mean
4°	Minimum	GLCM Mean	Mode	Minimum	Minimum
5°	Maximum	Assimmetry Polyg.	Maximum	Maximum	Maximum
6°	GLCM Mean	Length/Width	GLCM Mean	GLCM Mean	GLCM Mean
7°	GLCM 2°Ang. Moment	GLCM 2°Ang. Moment	Rectangular Fit	Length	Rectangular Fit
8°	Standard Deviation	GLCM Entropy	GLCM Correlat.	Rectangular Fit	GLCM Homog.
9°	Assimmetry Polyg.	Rectangular Fit	Density	Density	Compactness
10°	GLCM Homogeneity	Mean	Shape Index	Average Length Edges	Density
	Subset 6	Subset 7	Subset 8	Subset 9	Subset 10
1°	Minimum	GLCM Mean	Median	Median	Median
2°	Mean	Minimum	Mode	Minimum	Mean
3°	Median	Mean	Mean	Mode	Mode
4°	Standard Deviation	Median	Minimum	Mean	Minimum
5°	Mode	Mode	Maximum	Maximum	Maximum
6°	GLCM Dissimilarity	Maximum	GLCM Mean	Density	GLCM Mean
7°	GLCM Correlation	Assimmetry	Rectangular Fit	GLCM Mean	GLCM Correlation
8°	GLCM Mean	Compactness	GLCM Homog.	Rectangular Fit	Assimmetry Polyg.
9°	GLCM Contrast	GLCM Homogeneity	Elliptic Fit	Assimmetry Polyg.	Standard Deviation
10°	Density	Shape Index	Density	Standard Deviation	Assimmetry

■ Statistical ■ Textural ■ Geometrical

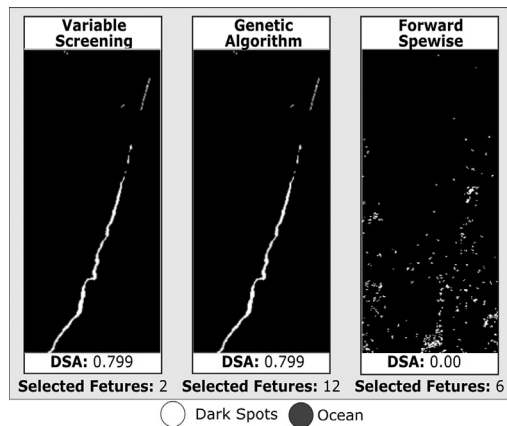


**Fig. 4.** Comparison between different feature selection methods, indicating the number of selected features by each method: (a) Variable Screening; (b) Genetic Algorithm; (c) Greedy Stepwise.

a single SAR scene, considered the easiest image to discriminate dark spots from the ocean. The selected features were clustered providing maps with two classes: ocean and dark spots. Fig. 4 provides the number of features selected, the clustering maps and the accuracy levels (DSA) for each method.

The accuracy levels were calculated using the metric Dark Spot Accuracy (DSA) (item 2.1), which considers as basis the clustering maps using the features selected by each tested method. The VS (Fig. 4a) and the GA (Fig. 4b) reached the same accuracy level (DSA = 0.799), while the GS had its accuracy equal zero (Fig. 4c). Therefore, in addition to the recommendation of the Variable Screening method for the data type used, it reached the same accuracy of the Genetic Algorithm method using fewer features.

#### 2.4.1. Feature selection results using the variable screening method

To assist the feature selection process a Principal Component Analysis (PCA) was done to identify the minimum number of features needed to maintain at least 90% of the dataset represen-

tativeness. The minimum number of Eigenvectors (features) indicated by the PCA for each subset ( $S_i$ ) [ $S_i: i \{1, \dots, 10\}$ ] was, respectively:  $S_1: 10$ ;  $S_2: 7$ ;  $S_3: 8$ ;  $S_4: 8$ ;  $S_5: 10$ ;  $S_6: 5$ ;  $S_7: 9$ ;  $S_8: 8$ ;  $S_9: 8$ ;  $S_{10}: 10$ . As a result, 10 features were indicated as the maximum number needed to maintain 90% of representativeness. Table 3 provides the chi-square ranking for the best 10 features per subset.

The best set of features selected as input for the dark spot detection systems is different, not only because of the chosen method, but also because of the particular characteristics of each SAR dataset acquired. Different meteo-oceanographic conditions, as well as different SAR sensors configuration, influence these results. Additionally, different attributes can be more or less important to improve the detection process, depending on the type of the dark spot - oil or look-alikes - and its characteristics: backscatter intensity, texture, size and geometry.

Although the recurrence of certain features was observed, the ranking of the 10 most important features was different for each subset. To define a set of pattern features to be used as input in the proposed system, the cumulative frequency was done to indicate the 10 first recurrent features selected by the chi-square, being: 1st) Median; 2nd) Mean; 3rd) Mode; 4th) Minimum; 5th) Maximum; 6th) GLCM Mean; 7th) Rectangular Fit; 8th) GLCM Homogeneity; 9th) Asymmetry of Polygons and; 10th) Density.

#### 2.5. Automatic and semi-automatic detection

Considering that the segmentation may under or over-segment the dark spots, an additional processing is necessary to merge (Step IV) the low backscatter regions in one single geometry. Thus, the clustering analysis can be performed using as input the features previously selected according to its statistical significance and order of importance.

In general, the clustering methods can be classified as (Breiman, Friedman, Olshen, & Stone, 1984; Han & Kamber, 2001; Mythili & Madhiya, 2014; Sharma & Borana, 2014): i) Partitioning; ii) Hierarchical; iii) Density-based; iv) Grid-based, and; v) Model-based. Partitioning and hierarchical methods are usually preferred for more generic implementations. A further analysis, comparing

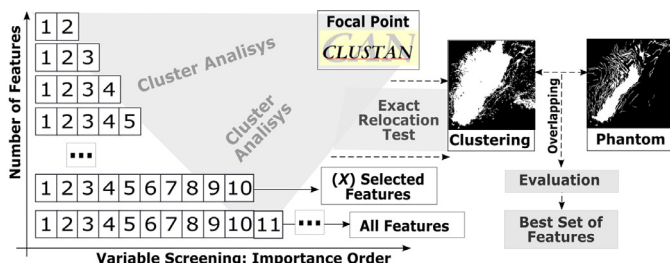


**Fig. 5.** Clustering method to find and validate the best set of features.

both automatic with semi-automatic efficient algorithms, are done to evaluate the existent trade-off and the advantages to build a hybrid system which is able to integrate supervised and unsupervised approaches using decision rules.

### 2.5.1. Automatic dark spot detection

The Focal Point algorithm, available in the Clustan software (Wishart, 2004), was used to perform the automatic clustering analysis. This algorithm uses a K-means partition method to cluster the data. Despite the K-means is simple to implement and recommended to process large datasets (Jain et al., 1999), it is sensitive to the initial partition, converging to different results at each new interaction.

The Focal Point (FP) was chosen because it assures the convergence, returning always to the same clusters through exact relocation tests. The FP is able to: *i*) test the sensitivity related to the initial partition order; *ii*) save the best solutions ordered by the best fit; *iii*) estimate the reproducibility of each solution; *iv*) remove outliers and intermediates, and; *v*) automatically re-weights the features (Wishart, 2004).

To evaluate the quality of the clusters and ensure the best result, the software uses the Euclidian Distance of Squares Sum ( $E_p$ ) between all members of the cluster  $p$  and its mean:

$$E_p = \sum_{i \in p} \sum_j \frac{(x_{ij} - \mu_{pj})^2}{f} \quad (2)$$

The notation uses  $j$  for the clustered feature,  $x_{ij}$  to represent the value of the feature  $j$  associated with the region  $i$ . The average in a given cluster  $p$  is represented by  $\mu_{pj}$ , and  $f$  is the total number of features considered. The FP reassigns the member of the initial clusters interactively to improve the Euclidian Squares Sum ( $E_p$ ). This process finishes when the  $E_p$  can no longer be reduced or the maximum number of interactions is reached.

The total  $E_p$  over all clusters is  $E = \sum_p E_p$  and FP will only move the region  $i$  from the cluster  $p$  to the cluster  $q$  when  $E_p - I + E_q + I < E_p + E_q$ . Therefore, the exact relocation test is the most important characteristic that differentiates FP from the other K-means implementations, assuring the same results in each convergence (Wishart, 2004).

The most effective set of features, able to return the best dark spot detection with a minimum number of features, was analyzed with the clustering results. To validate these results, the best set of features was processed by the FP considering as input: *i*) 10 selected features together, and; *ii*) 10 selected features, inserted gradually one by one, according to its order of importance, provided by the Chi-square cumulative frequency. The same analysis was done considering all 36 features as illustrated in Fig. 5.

The evaluation of the best set of features to detect dark spots was conducted by overlapping the dark spots designed in the Phantoms with the clustering results. The Dark Spot Accuracy (DSA) and the Maximum DSA (MaxDSA) obtained after the features combination were the metrics used.

Comparing the results, not necessarily the use of features with better discriminative capacity provides an effective result when clustered together with other features. Despite the feature Minimum being indicated before the feature Maximum, in the Chi-square ranking, this feature damaged the clustering results. This feature used as input alone or together with the feature Maximum returned low values of DSA in almost all subsets. To minimize this influence, the feature Minimum was excluded from the dataset and the 35 features and the 9 selected features were gradually inserted, considering the order of importance provided by the Chi-square ranking (Fig. 5).

**Table 4** and **Fig. 6** synthesizes all results obtained by the Focal Point: 1) Global: DSA obtained by the simultaneous insertion of the 9 features; 2) Maximum: MaxDSA obtained by the best features combination, considering a gradual insertion of the 9 features; 3) Number of features necessary to reach the MaxDSA; 4) Difference between (2) and (1); 5) Global: DSA obtained by the simultaneous insertion of 35 features; 6) Maximum: MaxDSA obtained by the best features combination, considering a gradual insertion of the 35 features; 7) Number of features necessary to reach the MaxDSA; 8) Difference between (6) and (5); 9) Difference between (1) and (5); 10) Difference between (2) and (6).

In most subsets, the DSA values considering the simultaneous clustering of 9 features (line 1: **Table 4**) were higher than those obtained for the simultaneous clustering of 35 features (line 5: **Table 4**), in average 0.39 for 9 features and 0.19 for 35 features.

The simultaneous processing of 35 features returned low accuracy levels, as seen in line 5 (**Table 4**), degrading the dark spot detection. As expected, the difference obtained in line 9 (**Table 4**) was considered statistically significant by the Wilcox test, with  $p$ -value equal 0.028. After a certain number of features, the inclusion of new variables into the model inserts poor or no information (Hughes, 1968).

Therefore, a reduced set of significant features was confirmed as better than the use of a large dataset, which includes non-representative features and may even degrade the performance of the clustering algorithms. In large datasets, the potential to discriminate dark spots including all features together is different of the sum of individual features.

These conclusions are reinforced by the comparison between the lines 2 and 6 (**Table 4**). The maximum accuracy values (MaxDSA), obtained considering the best set of 9 or 35 features, showed similar behavior when comparing subset to subset, indicating the importance to maintain only the significant variables in the model. In average, the MaxDSA obtained with the gradual insertion of 9 features was 0.43, while the one obtained through 35 features was 0.44. The Wilcox test confirmed, with a  $p$ -value of 0.086 (**Table 5**), that this difference presents no statistical significance, being irrelevant as seen at line 10, **Table 4**.

Comparing lines 1 and 2 at **Table 4** it is notable that, when the cluster analysis starts using as an input a previous selected dataset, the accuracy levels are improved. Consequently, the dark spot detection is not significantly influenced considering the insertion of all features simultaneously or gradually, as seen in line 4 at **Table 4**. In an opposite direction, at line 8 it is possible to verify the inclusion effect of all features without selection. In this case, combining only the best set of features is essential to improve the DSA.

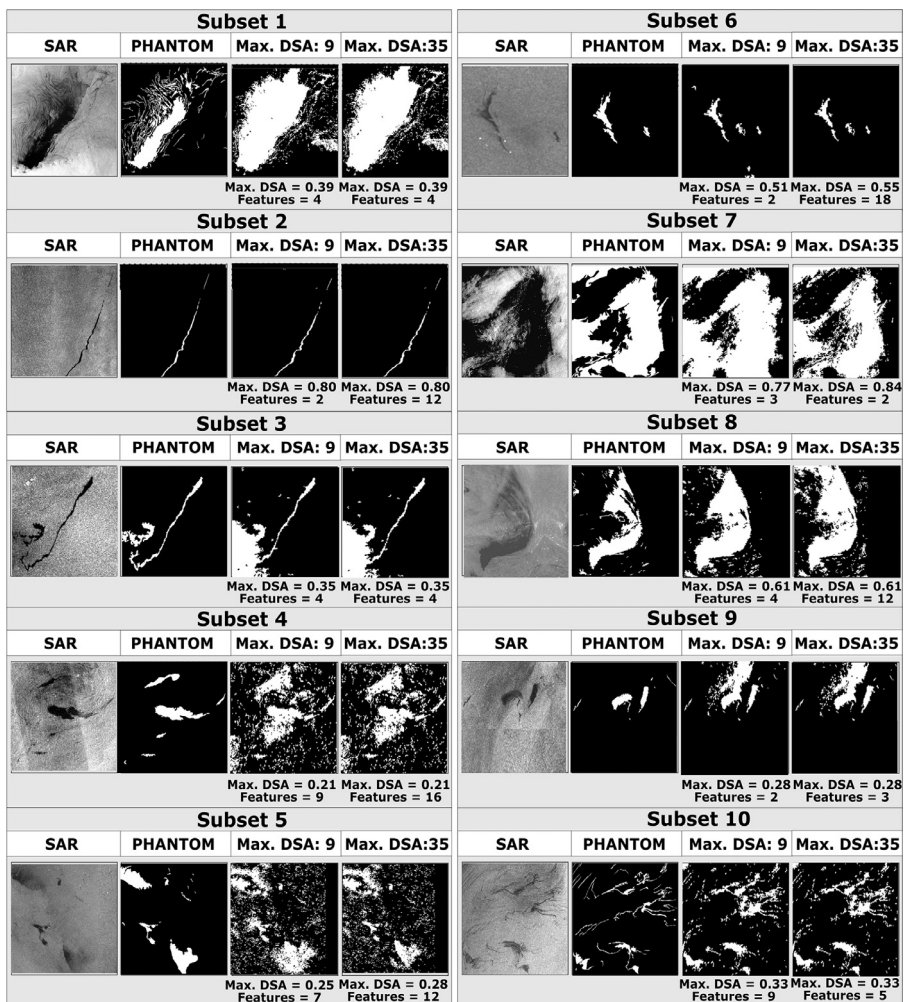
In most subsets it was possible to converge to the best solution using, as an input, a lower number of features, ranging between 2 and 4 (line 7: **Table 4**). The minimum number of features needed to achieve the MaxDSA was: *i*) 2 features for 3 subsets; *ii*) 3 features for 1 subset; *iii*) 4 features for 3 subsets; *iv*) 7 features for 1 subset, and; *v*) 9 features for 2 subsets.

Only for those cases where the MaxDSA was obtained using more than 4 features, the use of 2 or 3 features produced non-

**Table 4**

Clustering analysis results: focal point considering the 9 selected features and all 35 features.

9 FEATURES		SUBSETS										STATISTICS		
Focal Point		1	2	3	4	5	6	7	8	9	10	Mean	Median	Max
(1) DSA: 9 Features		0.35	0.80	0.35	0.22	0.25	0.33	0.44	0.56	0.24	0.33	0.39	0.34	0.80
(2) Max. DSA: Ranking of 9 features		0.39	0.80	0.35	0.22	0.25	0.51	0.77	0.61	0.28	0.33	0.45	0.37	0.80
(3) Number of Features: Max. DSA		4	2	4	9	7	2	3	4	2	9	5	4	9
(4) Difference: (2)-(1)		0.04	0.00	0.00	0.00	0.00	0.17	0.33	0.05	0.04	0.00	0.06	0.03	0.00
35 FEATURES		SUBSETS										STATISTICS		
Focal Point		1	2	3	4	5	6	7	8	9	10	Mean	Median	Max
(5) DSA: 35 Features		0.19	0.00	0.06	0.05	0.02	0.23	0.48	0.26	0.24	0.34	0.19	0.21	0.48
(6) Max. DSA: Ranking of 35 features		0.39	0.80	0.35	0.21	0.28	0.55	0.84	0.61	0.28	0.33	0.47	0.37	0.84
(7) Number of Features: Max. DSA		4	12	4	16	12	18	2	12	3	5	9	9	18
(8) Difference: (6)-(5)		0.20	0.80	0.29	0.16	0.26	0.32	0.37	0.35	0.04	0.01	0.28	0.16	0.37
(9) Difference: (1)-(5)		0.16	0.80	0.29	0.16	0.23	0.11	0.04	0.30	0.00	0.01	0.20	0.13	0.32
(10) Difference: (2)-(6)		0.00	0.00	0.00	0.00	0.04	0.04	0.07	0.00	0.00	0.00	0.01	0.00	0.04

**Fig. 6.** The focal point clustering results, indicating the number of features needed to obtain the Maximum DSA (MaxDSA) for the best set of predictor features among 9 and 35.

**Table 5**

Evaluation metrics calculated to the automatic and semi-automatic methods: DSA; In, and; Om.

DSA											Mean
	1	2	3	4	5	6	7	8	9	10	
Focal Point	0.39	0.80	0.35	0.15	0.24	0.51	0.44	0.61	0.25	0.10	0.38
Threshold	0.61	0.75	0.50	0.51	0.61	0.27	0.86	0.73	0.67	0.32	0.58
MaxVer	0.60	0.51	0.47	0.38	0.47	0.44	0.80	0.68	0.52	0.34	0.52
SVM	0.51	0.80	0.52	0.40	0.62	0.54	0.85	0.74	0.76	0.38	0.61
Inclusion	1	2	3	4	5	6	7	8	9	10	Mean
Focal Point	0.32	0.00	0.94	0.22	0.44	0.01	0.16	0.19	0.09	0.53	0.29
Threshold	0.28	0.07	0.04	0.15	0.24	0.02	0.05	0.30	0.10	0.23	0.15
MaxVer	0.02	0.01	0.00	0.05	0.00	0.01	0.05	0.01	0.02	0.05	0.02
SVM	0.17	0.00	0.00	0.05	0.03	0.00	0.08	0.02	0.01	0.03	0.04
Omission	1	2	3	4	5	6	7	8	9	10	Mean
Focal Point	0.03	0.12	0.00	0.27	0.19	0.39	0.02	0.02	0.20	0.10	0.13
Threshold	0.21	0.19	0.48	0.41	0.24	0.72	0.10	0.05	0.26	0.60	0.33
MaxVer	0.33	0.12	0.51	0.29	0.51	0.39	0.16	0.30	0.24	0.38	0.32
SVM	0.08	0.12	0.46	0.24	0.20	0.39	0.08	0.21	0.14	0.46	0.24

representative clusters. Therefore, there is a limit to reduce the dataset. A small number of features may not be enough to return representative clusters, as well as a great number of features may also degrade the dark spot detection.

Fig. 6 shows the spatial distribution of the MaxDSA obtained for the best combinations between 9 and 35 predictors, indicating the minimum number of features needed to achieve these accuracy levels. A comparison between the clusters confirmed that there were no relevant differences among the best combinations between 9 and 35 features.

Despite the automatic detection being possible using a reduced number of features, the spatialization of the dark spots detected was considered satisfactory ( $DSA \geq 0.50$ ) in only 4 subsets ( $S_2$ ;  $S_6$ ;  $S_7$ ;  $S_8$ ) (Fig. 6).

The main factor that contributed to these low accuracy levels was the rigorous criteria adopted to select the subsets and the reference Phantoms designed manually. Subsets including dark spots on different scales, with a different nature, occurring alone or simultaneously, well and badly-contrasted, contributed to simulate the real conditions observed in SAR data. As a benefit, it was possible to evaluate the difficulties and the real challenges related to the automatic dark spot detection, making it possible to verify situations where human intervention is needed to obtain acceptable accuracies.

As a result, the best number of pattern features needed to automate the system and to obtain the best accuracy levels was on average 5 (line 3 Table 4). In order to verify whether the use of 4 or 5 features would be statistically different, the Wilcox nonparametric test was performed. The  $p$ -value equal 0.68 indicated that there was no observed statistical significance between the DSA obtained using 4 or 5 features.

Therefore, the features recurrently selected to be used as input were the statistical features Median, Mean, Mode and Maximum, together with the textural feature GLCM Mean. These features were considered robust, because they were recursively selected in all subsets and validated with the clustering results.

The polygons clustered in subsets 2, 6, 7 and 8 were considered satisfactory with  $DSA > 0.5$  and could be used as input to the classification process in oil or lookalikes. However, the dark spots detected with  $DSA < 0.5$  would damage the performance of the classifiers, since a new feature extraction is needed using these geometries as a basis.

In this context, a hybrid approach, integrating semi-automatic techniques to detect dark spots was proposed as an alternative to obtain better geometries when the automatic procedures did not achieve satisfactory performances.

### 2.5.2. Semi-automatic dark spot detection

The supervised classifications were performed using the Maximum Likelihood (Maxver) and Support Vector Machine (SVM) algorithms, considering human intervention as the samples selection.

The Maxver was used because it is the most commonly used algorithm in supervised classifications. Despite this classifier being generally used for pixel-level processing, it was applied here with a region based approach, using the segmentation regions as processing units.

The SVM is indicated because it was evaluated as an efficient algorithm to separate oil from lookalikes (Bentz et al., 2007; Bentz et al., 2012; Brekke & Solberg, 2008; Coccioni, Corucci, Masini, & Nardelli, 2012; Matkan, Hajeb, & Azarakhsh, 2013; Mera, Bolon-Canedo, Cotos, Alonso-Betanzos, 2017; Mercier & Arduin, 2005; Xu et al., 2014) as well as to provide good results from complex and noisy SAR data.

The interactive OTSU thresholding (Otsu, 1979) was used considering a greater amount of human intervention than the other supervised methods. The goal was to simulate the interpreters' supervision in oil and lookalikes detection, considering that the ideal threshold is achieved interactively, selecting the best cut-off value to return clusters similar to the Phantoms. To process the classifications with Maxver and SVM, image files containing 5 bands [Median, Mean, Mode, Maximum and GLCM: Mean] were generated and spatialized among the segmented regions for each subset.

The scale factor - the only parameter required by Maxver - was defined as 255, according to the radiometric resolution of the SAR data in amplitude (8 bits). The SVM parameters were: i) kernel function as the Radial Basis Function (RBF); ii) penalty factor equal 100, not accepting levels of inaccuracy, and; iii) Gamma 0.2, equal to the inverse of the number of image bands (1/5).

The dark spots provided by the automatic and semi-automatic procedures were overlapped with the Phantoms, generating the evaluation metrics spatialized in Fig. 7 and available in

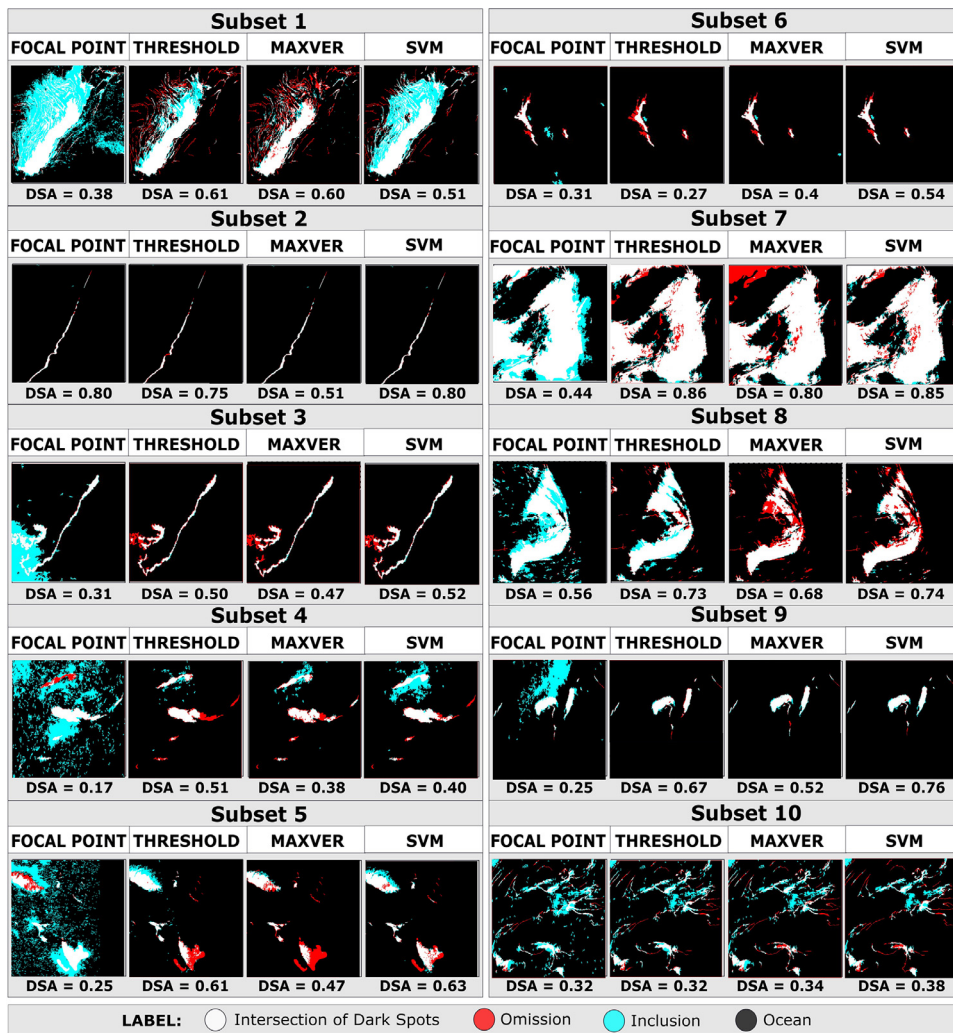


Fig. 7. Dark spots detection performed by automatic and semi-automatic algorithms.

**Table 5:** Dark Spot Accuracy (DSA); Inclusion (In), and; Omission (Om).

The qualitative and quantitative results indicated that the semi-automatic methods returned more representatives clusters and, consequently, better geometries. As expected, for the subsets containing well-defined and well-contrasted single dark spots, the results provided by the semi-automatic algorithms were equivalent to those provided by the automatic algorithm. This can be seen in subsets 2 and 6, which returned satisfactory DSAs.

The results obtained in the subsets 8 and 10 were also considered as similar, because all methods failed by including or omitting regions (see Table 5). For the subsets 3 and 9, the automatic performance was unsatisfactory because of high inclusion errors, decreasing the DSA values. This occurred because of the simultaneous presence of low wind intensities in the background. A similar effect was observed in subsets 1 and 10, where dark spots, typical for biogenic oils, with complex geometries and characterized by filamentous structures, were also influenced by the low wind intensities.

Subsets 4 and 5 presented better results using the semi-automatic algorithms. In this case, the FP inclusion error was higher than the other methods, increasing the noise level in the background. Subset 4 had imaging failures and subset 5 multiple types of dark spots in different scales occurring together, factors that corroborated the unsatisfactory performance of the FP.

Except for subsets 2 and 6, containing dark spots, which can be easily recognized, all methods failed including or excluding regions at different levels.

Considering that, the DSA decreases when the Inclusion or Omission errors increase, the FP had an inverse behavior when compared with the supervised approaches, providing more failure of inclusion (0.29) than omission (0.13), as seen in Table 5. As expected, the best performances were obtained by the supervised methods, indicating firstly the SVM algorithm with DSA in average equal 0.61, followed by Threshold (DSA = 0.58), Maxver (DSA = 0.52) and, finally, the FP with DSA in average of 0.38.

The results showed that, the decision rules are an interesting approach for complex SAR subsets, being able to indicate when human intervention is needed to improve the geometric accuracy. This approach is promising and represents a new method to make processing of large SAR datasets operational, providing results delivered in near real time with enough accuracy to assist the planning and execution of oil spills response actions (OSR).

## 2.6. Decision Rules: computational intelligence to integrate automatic and semi-automatic detection

To extract simple and compact rules able to indicate whether the SAR scenes need semi-automatic processing, the Classification and Regression Trees may be used. This is needed to create a de-

**Table 6**

Input features used by the classification and regression trees to generate the decision rules.

	$X_1 = \text{Dif. Median}$	$X_2 = \text{Dif. Mean}$	$X_3 = \text{Dif. Mode}$	$X_4 = \text{Dif. Maximum}$	$X_5 = \text{Dif. GLCM Mean}$	Clustering performance
Subset 1	0.23	0.20	0.21	0.12	0.23	US
Subset 2	0.33	0.35	0.31	0.22	0.42	S
Subset 3	0.41	0.32	0.45	0.23	0.34	US
Subset 4	0.10	0.10	0.09	0.1	0.40	US
Subset 5	0.08	0.09	0.06	0.09	0.43	US
Subset 6	0.22	0.31	0.28	0.10	0.43	S
Subset 7	0.11	0.12	0.11	0.15	0.37	US
Subset 8	0.28	0.22	0.28	0.15	0.27	S
Subset 9	0.29	0.16	0.27	0.14	0.38	US
Subset 10	0.36	0.32	0.35	0.14	0.40	S

cision rule to predict the behavior of the dependent feature ( $Y$ ), using as input predictor features ( $X$ ).

This approach provides a set of rules which propagate from the root, towards the nodes until the leaves, where: *i*) the root node contains the number of elements and predictor features ( $X$ ) used to estimate the rules; *ii*) the ramifications establish the binary partition criteria, according to the numerical attributes provided, and; *iii*) the leaves contain the number of elements, selected by the decision rule, to represent the classes indicated by the dependent feature ( $Y$ ) (Aggarwal, 2015; Breiman et al., 1984; Han & Kamber, 2001; Lixin, 2016; Sharma & Kumar, 2016).

The Classification and Regression Tree was performed considering as input the following features: *i*) one categorical dependent feature ( $Y$ ), and; *ii*) 5 new predictor metrics represented by the vector  $X$ , being  $X = \{X_1, \dots, X_5\}$ , which was calculated using the Focal Point output as the basis.

In the proposed model, the categorical dependent feature ( $Y$ ) was represented by the Dark Spot Accuracy (DSA) metric, indicating whether the automatic detection was Satisfactory (S:  $DSA \geq 0.50$ ) or Unsatisfactory (US:  $DSA < 0.50$ ).

At the end of the clustering, the Focal Point provides the average of the five (5) features for the regions clustered as dark spots and ocean. The new predictor features ( $X$ ) were calculated subtracting the means obtained for the clusters merged as ocean from those merged as dark spots. These metrics represent the distance between the clusters for the two classes, Dark Spots (DS) and Ocean (Oc), being: *i*)  $X_1 = \mu_{Oc} \text{ Median} - \mu_{DS} \text{ Median}$ ; *ii*)  $X_2 = \mu_{Oc} \text{ Mean} - \mu_{DS} \text{ Mean}$ ; *iii*)  $X_3 = \mu_{Oc} \text{ Mode} - \mu_{DS} \text{ Mode}$ ; *iv*)  $X_4 = \mu_{Oc} \text{ Maximum} - \mu_{DS} \text{ Maximum}$ , and; *v*)  $X_5 = \mu_{Oc} \text{ GLCM Mean} - \mu_{DS} \text{ GLCM Mean}$ . The new categorical and predictor features are presented in Table 6.

The objective was to find out decision rules to indicate whether the clustering results may be satisfactory (S) or unsatisfactory (US), leading the SAR scenes to the supervised approach when the rules indicate an un-satisfactory performance for the automatic detection.

The ten (10) SAR scenes previously processed were used to extract the decision rule and the other two (2) new scenes were considered to validate the decision rule, aiming to verify its feasibility to integrate the human intervention by the semi-automatic approach when needed.

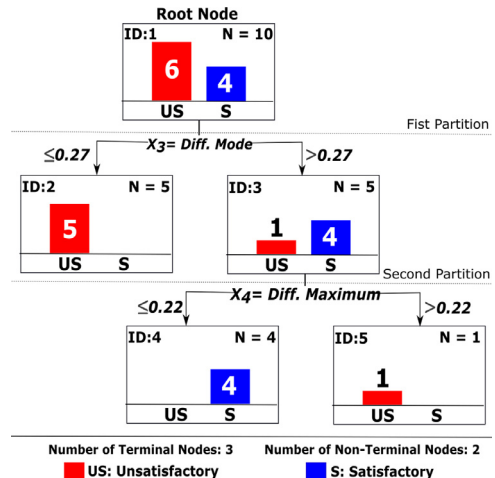


Fig. 8. Classification and Regression Tree, indicating the satisfactory and unsatisfactory scenes.

**Table 7**

Automatic dark spots detection results, considering the aforementioned evaluation metrics.

Validation	DSA	Int	Om	In	Clustering performance
Subset A	0.46	0.93	0.07	0.10	US
Subset B	0.50	0.88	0.12	0.08	S

As a result, one structure derived from the root node was composed by 2 partitions (Fig. 8), originating 2 nodes and 3 leaves. The size of the root node was equal to the number of the input components, and equivalent to the number of the subsets (10).

The first partition rule, based on the  $X_3$  feature [difference between Mode], subdivided 5 components classified as US to the left branch and the other 5 ones to the right branch, 1 being classified as US and 4 as S. The second partition rule, based on the feature  $X_4$  [Difference between Maximum], subdivided the 5 remaining components in 2 new branches, the left with 4 S and the right with 1 US (Fig. 8).

The classification and regression tree returned one compact and simple decision rule, which corresponds with the results obtained by the clustering analyses, confirming that only 4 subsets gave satisfactory results for the dark spots detection. The tree with the decision rules obtained is available in Fig. 8.

To validate the decision rule, 2 other SAR subsets were processed considering the parameters defined in the previous steps: *i*) Pre-processing: pixel spacing 100 m and filter Lee  $3 \times 3$ ; *ii*) Segmentation with ISOSEG/SPRING: minimum area 25 pixels and similarity threshold equal 4; *iii*) Extraction of the 5 selected features: Median, Mean, Mode, Maximum and GLCM Mean; *iv*) Dark spot detection using the Focal Point clustering algorithm.

The results were checked to validate whether the automatic dark spots detection was considered satisfactory (S) or unsatisfactory (US). Phantoms were designed to extract the evaluation metrics. Table 7 provides the evaluation metrics to the automatic detection: Dark Spot Accuracy (DSA); Fraction of Intersection (Int); Inclusion (In); Omission (Om), and; clustering performance.

The automatic performance obtained by the Focal Point was considered non-satisfactory ( $DSA < 0.50$ ) to the validation subset A, which returned a noisy appearance in its background (Fig. 9).

The scalability of the dark spots, occurring with different dimensions in the subset A, was a factor influencing these results.

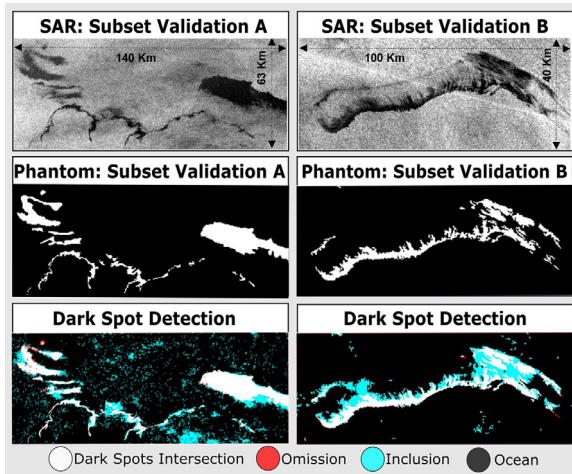


**Fig. 9.** Original SAR data, Phantoms and automatic dark spot detection overlapping used to calculate the evaluation metrics.

**Table 8**  
Metrics to decision rule validation.

Validation	X <sub>2</sub> = Diff. Mode	X <sub>3</sub> = Diff. Maximum	DSA	Clustering performance
Subset A	0.26	0.10	0.46	US
Subset B	0.35	0.18	0.50	S

The parameter of Minimum Area, defined as 25 pixels, was used to permit that, even small dark spots, could be detected by the clustering algorithm. However, the excess of small-segmented regions in the background produced a noisier appearance of the ocean. Additionally, the influence of the low wind intensities occurring in this scene confirms this result.

The inclusion error obtained in the validation subset A (0.10) was higher than the one obtained in the validation subset B (0.08), confirming that the automatic detection merged ocean regions erroneously as dark spots (Table 7).

The automatic performance provided by the Focal Point in the validation subset B was considered satisfactory with DSA = 0.50. Visually the dark spots were well detected by the clustering algorithm with low noise in the background. However, it is noticeable that the rigor applied to design the Phantom borders manually, induced a higher inclusion error around the edges. These comments can be seen in the maps available in Fig. 9, highlighting the evaluation metrics calculated.

The 2 new metrics, X<sub>3</sub> [ $\mu_{\text{Oc}} \text{ Mode} - \mu_{\text{DS}} \text{ Mode}$ ] and X<sub>4</sub> [ $\mu_{\text{Oc}} \text{ Maximum} - \mu_{\text{DS}} \text{ Maximum}$ ], presented in Table 8 were used to validate the decision rule. As expected, the metrics confirmed the DSA obtained for each subset, indicating that the dark spot detection was un-satisfactory ( $X_3 \leq 27$ ) in subset A and satisfactory ( $X_3 > 27$  and  $X_4 \leq 22$ ) in the subset B.

Therefore, the decision rule confirmed the DSA levels obtained by each subset, indicating that subset B can be processed automatically while subset A must integrate the semi-automatic procedure to improve the dark spot detection.

The flowchart integrating all steps of the intelligent hybrid system proposed is showing in Fig. 10. The results present the potential of the decision rules to assist the dark spot detection, indicating situations where human intervention is required to produce representative geometries with acceptable noise level in the background.

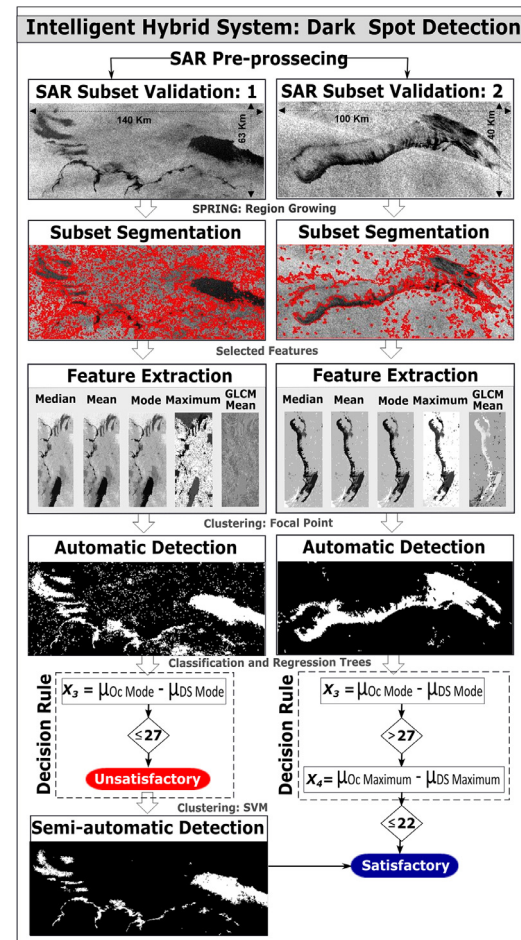


**Fig. 10.** Intelligent hybrid system proposed for dark spot detection, integrating automatic and semi-automatic algorithms.

### 3. Conclusions

An intelligent hybrid system using decision rules to integrate automatic and semi-automatic procedures for dark spots detection was proposed, tested and validated. As a novelty, the feature extraction and selection - applied to improve the classification process in oil or look-alikes - was applied for the dark spot detection. For this purpose, 36 statistical, textural and geometrical features were extracted and selected, finding an optimal number of these inputs to automate the proposed system.

The feature selection indicated the statistical relevant ones as the most related with the dependent attribute named Phantom Class (PC), enforcing its better potential to contribute to the dark spot detection. The results obtained proved that the feature selection is essential to improve the detection capability, indicating the importance to keep only the significant variables in the model. The dark spot accuracy levels (DSA) always improved when the cluster analysis was performed using previous selected dataset instead of all features together.

There is a limit to reduce the attribute space and a small number of features may not be enough to return representative clusters as well as - considering the Hughes effect - the combination of a great number of features may also degrade the dark spot detection. The studies conducted with 10 SAR scenes, indicated 5 pattern features as enough to automate the system using the Focal Point algorithm, which returns the same geometries for each new interaction.

The semi-automatic methods returned more representatives clusters and, consequently, more accurate geometries. The semi-automatic methods erred more excluding regions that would be dark spots, while the automatic method erred more including oceanic regions and increasing the effective area of the dark spots.

From an operational point of view, even inaccurate geometries detected for complex dark spots, would be useful to plan flight surveillances when needed. However, they could not be useful as input to the automatic classification phase. The cumulative feedback of inaccurate geometries inside of knowledge databases used to recognize patterns in large datasets, might propagate errors, and therefore not recommended. In particular, all new extracted features, would be confronted with the previous knowledge by the decision rules.

For well-defined and well-contrasted dark spots, the performance of the automatic and semi-automatic methods were equivalent. Nevertheless, the rigorous criteria adopted to select the SAR scenes confirmed that a fully automatic method might not provide acceptable accuracies in all cases, particularly when complex dark spots with low contrast are present. In these cases, the integration of the human intervention, using the semi-automatic procedures, is recommended to obtain acceptable geometric accuracy for the classification phase.

The SAR scenes used to validate the system showed the potential of the decision rules to automate the dark spot detection, confirming situations where human intervention was needed through a hybrid approach. This architecture would allow a quick emission of alerts when suspected oil spills are identified using the automatic method. However, the system provides - at the same time - a quality control to indicate when the semi-automatic procedure is needed to improve the accuracy of the dark spot detection.

The classification and regression tree returned a compact and simple rule for single polarization modes (VV- HH), acquired in C Band. To improve the quality of the rules, being successfully applied for any SAR data, it is recommended to follow up this study by considering data acquired from different sensors, using different bands and polarization modes. This diversity of data requirements will provide options to extract and investigate the contribution of new features applied to dark spots detection.

Another important point to investigate would be the potential of the fully polarimetric SAR data (PolSAR) to deliver new features to improve the dark spot detection. Recent studies using several polarimetric attributes, highlighted the potential of the PolSAR data to detect different types of oils, discriminating between mineral and biological ones (Bandiera et al., 2014; Genovez et al., 2017; Matkan et al., 2013; Migliaccio et al., 2015; Salberg, Ølserberg, & A. H., 2014; Skrunes, Brekke, & Torbjørn, 2013). These type of data could improve not only the classification of oil or look-alikes, but also the dark spot detection.

In this context, considering the many factors of interference that may make dark spot detection with SAR data difficult, the proposal of an intelligent hybrid system constitutes an interesting and important approach. This system would integrate the benefits of each method, ensuring the quality of the classification phase when fully automatic procedures do not return satisfactory results.

## Acknowledgements

The authors are grateful to Research Center of Petrobras (CEN-PES/AMA) for providing SAR data and to CNPq for granting to projects #303752/2013-0 and #314248/2014-5. The Pollution Control and Aero-medical Rescue of Petrobras (E&P-SERV/CPRA) for the operational point of view, as well as the field truth used to confirm the different dark spots detected. Thank to Dr. Hermann Kux by improving the manuscript and to the Transfer Technology Cen-

ter of COPPE/UFRJ (NTT/UFRJ), together with the Digital Image Processing Division of INPE (DPI/INPE), by the expertise provided to support all issues related to this research.

## References

- Aggarwal, C. C. (2015). *Data mining*. The Textbook Springer International Publishing. doi:[10.1007/978-3-319-14142-8](https://doi.org/10.1007/978-3-319-14142-8).
- Angiuli, E., Frate, F., & Salvatori, L. (2006). *Neural networks for oil spill detection using ERS and ENVISAT imagery* . [online] [http://earth.esa.int/workshops/seasar2006/proceedings/papers/s54\\_ang.pdf](http://earth.esa.int/workshops/seasar2006/proceedings/papers/s54_ang.pdf).
- API: American Petroleum Institute (2013). *Remote sensing in support of oil spill response: Planning guidance* (p. 1144). USA: Washington, DC. Tech. Rep. no.
- Bandiera, F., Masciullo, A., & Ricci, G. A. (2014). Bayesian approach to oil slicks edge detection based on SAR data. *IEEE Transactions On Geoscience and Remote Sensing*, 52 Digital Object Identifier. doi:[10.1109/TGRS.2013.2267594](https://doi.org/10.1109/TGRS.2013.2267594).
- Bentz, C., Ebecken, N. F., & Politano, A. T. (2007). Automatic recognition of coastal and oceanic environmental events with orbital radars. *IEEE International Geoscience and Remote Sensing Symposium*, 1, 914–916 Barcelona. doi:[10.1109/IGARSS.2007.4422946](https://doi.org/10.1109/IGARSS.2007.4422946).
- Bentz, C., M., Politano, A. T., & Ebecken, N. F. F. (2012). Classification of oil spills and meteo-oceanographic events detected in SAR images. Geographic object-based image analysis. In *Fourth international conference on geographic object-based image analysis-GEOBIA, Rio de Janeiro, Brazil. Proceedings of the 4th GEOBIA* (pp. 618–621).
- Bins, L., Fonseca, L., & Erthal, G. (1996). Satellite imagery segmentation: A region growing approach. In *VIII Brazilian symposium on remote sensing*. São José dos Campos, BR: INPE.
- Bjerde, K. W., Solberg, A. H. S., & Solberg, R. (1993). Oil spill detection in SAR imagery. *Proceedings of IGARSS'93*, 3, 943–945.
- Brekke, C., & Solberg, A. H. S. (2005). Oil spill detection by satellite remote sensing – Review. *Remote Sensing of Environment*, 95, 1–13.
- Brekke, C., & Solberg, A. (2008). Classifiers and confidence estimation for oil spill detection in ENVISAT ASAR images. *IEEE Geoscience and Remote Sensing Letters*, 5(1) Digital Object Identifier. doi:[10.1109/LGRS.2007.907174](https://doi.org/10.1109/LGRS.2007.907174).
- Breiman, L., Friedman, J. H., Olshen, R. A., & Stone, C. J. (1984). *Classification and regression trees*. Monterey, CA: Wadsworth & Brooks/Cole Advanced Books & Software.
- Câmara, G., Cartaxo, R. M. S., Freitas, U. M., & Garrido, J. (1996). SPRING: Integrating remote sensing and GIS with object-oriented data modelling. *Computers and Graphics*, 20(3), 395–403.
- Chang, L., Cheng, C. M., & Tang, Z. S. (2005). An automatic detection of oil spills in SAR images by using image segmentation approach. *IEEE* [online] <http://ieeexplore.ieee.org/iel5/10226/32596/01525287.pdf?arnumber=1525287>.
- Chehresa, S., Amirkhani, A., Rezaie, G., & Mosavi, M. (2016). Optimum features selection for oil spill detection in SAR image. *Journal of the Indian Society of Remote Sensing*, 44(5), 775–787. doi:[10.1007/s12524-016-0553-x](https://doi.org/10.1007/s12524-016-0553-x).
- Calabresi, G., Del Frate, F., Lichtenegger, J., Petrocchi, A., & Trivero, P. (1999). Neural networks for the oil spill detection using ERS-SAR data. In *Proceedings of the international geoscience and remote sensing symposium (IGARSS'99)*: 1 (pp. 215–217). Pisacaway, USA: Hamburg.
- Cococcioni, M., Corucci, L., Masini, A., & Nardelli, F. (2012). SVME: An ensemble of support vector machines for detecting oil spills from full resolution MODIS images. *Ocean Dynamics*, 62, 449–467. doi:[10.1007/s10236-011-0510-8](https://doi.org/10.1007/s10236-011-0510-8).
- Published by Definiens Definiens Professional 5. (2006). In *Trappentreus Ag (Ed.). Reference book*: 1. Germany: München. Published by Definiens.
- Del Frate, F., Petrocchi, A., Lichtenegger, J., & Calabresi, G. (2000). Neural networks for oil spill detection using ERS-SAR Data. *IEEE Transactions On Geoscience And Remote Sensing*, 38(5) Publisher Item Identifier S 0196-2892(00)08910-5.
- Duda, R., Hard, P. E., & Stork, D. G. (2000). *Pattern classification* (2nd ed.) (p. 680). Wiley, ISBN: 978-0-471-05669-0.
- Engelhardt, F. R. (1999). Remote sensing for oil spill detection and response. *Pure and Applied Chemistry*, 71(1), 103–111.
- Espedal, H. A., & Wahl, T. (1999). Satellite SAR oil spill detection using wind history information. *International Journal of Remote Sensing*, 20(1), 49–65.
- Fingas, M., & Brown, C. (2014). Review of oil spill remote sensing. *Marine Pollution Bulletin*, 83(1), 9–23.
- Fiscella, B., Giancaspro, A., Nirchio, F., Pavese, P., & Trivero, P. (2000). Oil spill detection using marine SAR images. *International Journal of Remote Sensing*, 21(18), 3561–3566.
- Gade, M., Alpers, W., Hünerfuss, H., Wismann, V. R., & Lange, W. G. (1998). On the reduction of radar backscatter by oceanic surface films: Scatterometer measurements and their theoretical interpretation. *Remote Sensing of Environment*, 66(1), 52–70.
- Galland, F., Réfrégier, P., & Germain, O. (2004). Synthetic aperture radar oil spill segmentation by stochastic complexity minimization. *IEEE Geoscience and Remote Sensing Letters*, 1(4), 295–299.
- Garcia-Pineda, O., MacDonald, I., Hu, C., Svejkovsky, J., Hess, M., Dukhovskoy, D., et al. (2013). Detection of floating oil anomalies from the deepwater horizon oil spill with synthetic aperture radar. *Oceanography*, 26(2), 124–137.. <http://dx.doi.org/10.5670/oceanog.2013.38>.
- Gasull, A., Fabregas, X., Jimenez, J., Marques, F., Moreno, V., & Herrero, M. (2002). Oil spills detection in SAR images using mathematical morphology. *Proceedings of the EUSIPCO'2002, Toulouse, France*, 1, 25–28.

- Genovez, P. (2010). SAR image classification and segmentation for dark spot detection in oceanic petroleum exploration' and production areas. Ph.D. Dissertation, Federal University of Rio de Janeiro (COPE/UFRJ) [online]: <http://www.coc.ufrj.br/index.php/teses-de-doutorado/154-2010/1239-patricia-carneiro-genovez#download>.
- Genovez, P., Freitas, C., Sant'Anna, S., Bentz, C., & Lorenzetti, J. A. (2017). Oil slicks detection from polarimetric data using stochastic distances between complex wishart distributions. *IEEE Journal of Selected Topics in Applied Earth Observations and Remote Sensing*, 10(2), 463–477. doi:10.1109/JSTARS.2016.2628325.
- Han, J., & Kamber, J. (2001). *Data mining: Concepts and techniques*. United States: Academic Press.
- Hang, L. M., & Dinh, D. N. (2009). Oil spill detection and classification by ALOS PALSAR at Vietnam East Sea. In *7th FIG regional conference spatial data serving people: Land governance and the environment—building the capacity* (pp. 19–22). Hanoi: Vietnam.
- Haralick, R., Shanmugan, K., & Dinstein, I. (1973). Textural features for image classification. *IEEE Transactions on Systems, Man and Cybernetics*, 3(1), 610–621.
- Holt, B. (2004). SAR imaging of ocean surface. Chapter 2 in synthetic aperture radar marine user's manual, Organized by C. R. Jackson & J. R. Apel National Oceanic and Atmospheric Administration – NOAA.
- Hughes, G. (1968). On the mean accuracy of statistical pattern recognizers. *IEEE Transactions On Information Theory*.
- Indregard, M., Solberg, A., & Clayton, P. (2004). D2-report on benchmarking oil spill recognition approaches and best practice. Tech. rep., Oceanides project, European Commission, Archive no. 04-10225-A-Doc, Contract No: EVK2-CT-2003-00177.
- IPIECA (International petroleum industry environmental conservation association) and OGP (International association for oil and gas producers). (2014). An Assessment of Surface Surveillance Capabilities for Oil Spill Response using Airborne Remote Sensing. London, U.K., 86p. (Tech. Rep.: PIL-4000-38-TR-1.0).
- Jain, A. K., Murty, M. N., & Flynn, P. J. (1999). Data clustering a review. *ACM Computing Surveys*, 31(3), 264–323.
- Jing, F., He, C., FuKun, B., Jun Xia, L., & Hang, W. (2014). Detection of oil spills in a complex scene of SAR imagery. *Science China Technological Sciences*, 57(11), 2204–2209. doi:10.1007/s11431-014-5643-9.
- Karathanassi, V., Topouzelis, K., Pavlakis, P., & Rokos, D. (2006). An object-oriented methodology to detect oil spills. *International Journal of Remote Sensing*, 27, 5235–5251.
- Keramitsoglou, I., Cartalis, C., & Kiranoudis, C. (2006). Automatic identification of oil spills on satellite images. *Environmental Modelling & Software*, 21, 640–652.
- Konik, M., & Bradtke, K. (2016). Object-oriented approach to oil spill detection using ENVISAT ASAR images. *ISPRS Journal of Photogrammetry and Remote Sensing*, 118, 37–52.
- Kubat, M., Holte, C., & Matwin, S. (1998). Machine learning for detection of oil spills in satellite Radar images. *Machine Learning*, 30(2–3), 195–215.
- Lehmann, E. L., & Joseph, P. R. (2005). *Testing statistical hypotheses* ((3 ed.)). New York: Springer.
- Liu, H., & Setiono, R. (1995). Chi2: Feature selection and discretization of numeric attributes. In *Proceedings of the 7th IEEE international conference on tools with artificial intelligence* (pp. 388–391). <http://www.icsc.nus.sg/~liuh/tai95.ps>.
- Leifer, I., Lehr, W. J., Simecek-Beatty, D., Bradley, E., Clark, R., Dennison, P., et al. (2012). State of the art satellite and airborne marine oil spill remote sensing: Application to the BP deepwater horizon oil spill. *Remote Sensing of Environment*, 124, 185–209.
- Lixin, F. (2016). Accurate robust and efficient error estimation for decision trees. In *Proceedings of the 33rd international conference on machine learning* New York, NY, USA, 48.
- Lopez, L., Moctezuma, M., & Parmiggiani, F. (2005). Oil spill detection using GLCM and MRF. IEEE [online] <http://ieeexplore.ieee.org/iel5/10226/32597/01526349.pdf&number=1526349>.
- Marghany, M. (2014). Utilization of a genetic algorithm for the automatic detection of oil spill from RADARSAT-2 SAR satellite data. *Marine Pollution Bulletin*, 89, 20–29. <http://dx.doi.org/10.1016/j.marpolbul.2014.10.041>.
- Matkan, A., Hajeb, M., & Azarakhsh, Z. (2013). Oil spill detection from SAR image using SVM based classification. International archives of the photogrammetry, Remote Sensing and Spatial Information Sciences, 5–8 Volume XL-1/W3, 2013. SMPR 2013.
- Mera, D., Cotos, J. M., Varela-Pet, J., Rodríguez, P. G., & Caro, A. (2014). Automatic decision support system based on SAR data for oil spill detection. *Computers & Geosciences*, 72, 184–191. <http://dx.doi.org/10.1016/j.cageo.2014.07.015>.
- Mera, D., Bolon-Canedo, V., Cotos, J. M., & Alonso-Betanzos, A. (2017). On the use of feature selection to improve the detection of sea oil spills in SAR images. *Computers & Geosciences*, 100, 166–178. <http://dx.doi.org/>. doi:10.1016/j.cageo.2016.12.013.
- Mercier, G., & Arduin, G. (2005). *Unsupervised oil slick detection by SAR imagery using support vector machines* [online] <http://perso.enst-bretagne.fr/~mercierg/articles/2005/mercier.igarss05.pdf>.
- Migliaccio, M., Nunziata, F., & Buono, A. (2015). SAR polarimetry for sea oil slick observation. *International Journal of Remote Sensing*, 36(12), 3243–3273. doi:10.1080/01431161.2015.1057301.
- Mythili, S., & Madhiya, E. (2014). An analysis on clustering algorithms in data mining. *International Journal of Computer Science and Mobile Computing*, 3(1), 334–340.
- Montali, A., Giacinto, G., Migliaccio, M., & Gambardella, A. (2006). Supervised pattern classification techniques for oil spill classification in sar images: Preliminary results. In *Proceedings of SEASAR*. Italy.
- Navulur, K. (2007). *Multispectral image analysis using the object-oriented paradigm*. London - New York: CRC Press Taylor & Francis Group 6000 Broken Sound Parkway.
- Otsu, N. (1979). A threshold selection method from gray-level histograms. *IEEE Transactions on Systems, Man, and Cybernetics*, 9(1), 62–66 1979.
- Pelizzari, S., & Dias, J. M. B. (2003). Bayesian adaptative oil spill segmentation of SAR images via graph cuts. [online] [http://earth.esa.int/workshops/seasar2006/participants/256/paper\\_SoniaPelizzari\\_SEASAR2006\\_final.pdf](http://earth.esa.int/workshops/seasar2006/participants/256/paper_SoniaPelizzari_SEASAR2006_final.pdf).
- Qian, W., Shu, W., & Zhang, C. (2016). Feature selection from the perspective of knowledge granulation in dynamic set-valued information system. *Journal of Information Science and Engineering*, 32, 783–798.
- Salberg, A., ØSolberg, Rudjord, & A. H. , S. (2014). Oils spill detection in hybrid-polarimetric SAR images. *IEEE Transactions on Geoscience and Remote Sensing*, 52(10), 6521–6533. doi:10.1109/TGRS.2013.2297193.
- SeaSAR. (2010). Workshop, SEASAR 2010, entitled Advances in SAR Oceanography from ENVISAT, ERS and ESA third party missions, which will be hosted at ESA ESRIN in Frascati, Italy, 25–29 Jan.
- Sharma, M., & Borana, K. (2014). Clustering in data mining: A brief review. *International Journal of Core Engineering & Management (IJCEM)*, 1(5), 117–126.
- Sharma, H., & Kumar, S. (2016). A survey on decision tree algorithms of classification in data mining. *International Journal of Science and Research (IJSR)*, 5(4), 2094–2097.
- Silva, M. P. S., Câmara, G., Souza, R. C. M., Valeriano, D. M., & Escada, M. I. S. (2005). Mining patterns of change in remote sensing image databases. *The fifth IEEE international conference on data mining*. Houston.
- Singha, S., Velotto, D., & Lehner, S. (2014). Near real time monitoring of platform sourced pollution using TerraSAR-X over the North Sea. *Marine Pollution Bulletin*, 86, 379–390.
- Skrunes, S., Brekke, C., & Torbjørn, E. (2013). Characterization of marine surface slicks by Radarsat-2 Multi-polarization features. In *Proceedings: IEEE transactions on geoscience and remote sensing* (pp. 5117–5120).
- Skrunes, S., Brekke, C., Eltoft, T., & Kudryavtsev, V. (2015). Comparing near-coincident C- and X- Band SAR acquisitions of marine oil spills. *IEEE Transactions on Geoscience and Remote Sensing*, 53(4), 1958–1975.
- Solberg, R., & Theophilopoulos, N. A. (1997). Envisys-A solution for automatic oil spill detection in the Mediterranean. In *Proceedings of 4th thematic conference on remote sensing for marine and coastal environments* (pp. 3–12). Ann Arbor, Michigan: Environmental Research Institute of Michigan.
- Solberg, A. H. S., Dokken, S. T., & Solberg, R. (2003). Automatic detection of oil spills in Envisat, Radarsat and ERS SAR images. In *Proceedings of the international geoscience and remote sensing symposium*, Toulouse, France. Pisacataway, USA: IEEE.
- Solberg, A., Clayton, P., & Indregard, M. (2005). D2 –Report on benchmarking oil spill recognition approaches and best practice. Kongsberg Satellite Services–Norway Archive No.: 04-10225-A-Doc, Issue/Revision, 2, 1.
- Stathakis, D., Topouzelis, K., & Karathanassi, V. (2006). Large-scale feature selection using evolved neural networks. In Lorenzo Bruzzone (Ed.), *Proceedings of SPIE, image and signal processing for remote sensing XII*. In *SPIE bellingham Wash. ETAT-S-UNIS: Stockholm: 13–14* (p. 6365). Sweden. September.
- Taravat, A., & Oppelt, N. (2014). Adaptive weibull multiplicative model and multilayer perceptron neural networks for dark-spot detection from SAR imagery. sensors, 22798–22810; doi:10.3390/s141222798
- Topouzelis, K., Karathanassi, V., Pavlakis, P., & Rokos, D. (2007). Detection and discrimination between oil spills and look-alike phenomena through neural networks. *ISPRS J. Photogrammetry and Remote Sensing*, 62(9A), 264–270.
- Topouzelis, K. N. (2008). Oil spill detection by SAR images: Dark formation detection, feature extraction and classification algorithms. *Sensors*, 8(10), 6642–6659. doi:10.3390/s8106642.
- Topouzelis, K., Stathakis, D., & Karathanassi, V. (2009). Investigation of genetic algorithms contribution to feature selection for oil spill detection, intern. *Journal of Remote Sensing*, 30(3), 611–625.
- Topouzelis, K., & Psyllos, A. (2012). Oil spill feature selection and classification using decision tree forest on SAR image data, in *ISPRS Journal of Photogrammetry and Remote Sensing*, vol. 68(1), 135–143.
- Vanaja, S., & kumar, R. K. (2014). Analysis of feature selection algorithms on classification: A survey. *International Journal of Computer Applications*, 96(17), 0975–8887.
- Wishart, D. (2004). Focal point clustering user guide. Published by Clustan limited, Edinburgh Road, Scotland, (2nd ed.).
- Xu, L., Li, J., & Brenning, A. (2014). A comparative study of different classification techniques for marine oil spill identification using RADARSAT-1 imagery. *Remote Sensing of Environment*, 141, 14–23.
- Zheng, Y., Dong, H., Jiang, Q., & Li, J. (2005). A modified FCM-based algorithm for oil spill detection in SAR images. *Environmental Informatics Achieves*, 3, 346–351.